Peer-reviewed version available at Sensors 2018, 18, 2533; doi:10.3390/s18082533

Article

Optimal design of electromagnetically actuated MEMS cantilevers

Paolo Di Barba[1], Teodor Gotszalk[2], Wojciech Majstrzyk[2], Maria Evelina Mognaschi[1]*, Karolina Orłowska[2], Sławomir Wiak[3], Andrzej Sierakowski[4]

[1] Dept. of Electrical, Computer and Biomedical Engineering, University of Pavia, Italy; {paolo.dibarba, eve.mognaschi}@unipv.it
[2] Faculty of Microsystem, Electronics and Photonics, Wrocław University of Science and Technology, Wrocław, Poland; {teodor.gotszalk, wojciech.majstrzyk, karolina.orlowska}@pwr.edu.pl
[3] Institute of Mechatronics and Information Systems, Łódź University of Technology, Łódź, Poland; slawomir.wiak@p.lodz.pl
[4] Institute of Electron Technology, Warsaw, Poland; asierak@ite.waw.pl

* Correspondence: eve.mognaschi@unipv.it; Tel.: +39-0382-985-785

Abstract: In this paper we present the numerical and experimental results of a design optimization of electromagnetic cantilevers. In particular, a cost-effective technique of evolutionary computing enabling the simultaneous minimization of multiple criteria is applied. A set of optimal solutions are subsequently fabricated and measured. The designed structures are fabricated in arrays, which makes the comparison and measurements of the sensor properties reliable. The microfabrication process, based on the silicon on insulator (SOI) technology, is proposed in order to minimize parasitic phenomena and enable efficient electromagnetic actuation. Measurements on the fabricated prototypes assessed the proposed methodological approach.

Keywords: electromagnetically actuated cantilevers, nanometrology, multiobjective optimisation, active cantilevers, SOI-based prototyping

1. Introduction

Micro-electromechanical systems (MEMS) are the micromachines containing movable parts whose deflection is controlled and detected electronically. In general MEMS are manufactured using technologies applied in microelectronics which makes it possible to fabricate in the batch process devices of various functions and properties.

The critical physical dimensions of MEMS devices, to which belong simple structures having no moving elements and extremely complex electromechanical systems with elements actuated and controlled by the integrated microelectronics, can vary from several microns to several millimeters. In a natural way the MEMS technology merges at the nanoscale into nanoelectromechanical-systems (NEMS). To MEMS devices belong among others the so called supported cantilevers, whose elasticity can be described with relatively high accuracy using simple models. Moreover, the variety of possible applications is very broad ranging from scanning probe microscopy (SPM) to sensing systems applied in biochemistry and biotechnology [1]. In all the aforementioned applications the cantilever static or resonance deflection is detected to follow the phenomena of interest. Optical and electrical techniques, which can be applied in single or array cantilever (sensor) operation, enable monitoring of thermomechanical noise structure vibration. It should be however mentioned, that the full interoperability of the cantilever system can only be obtained when the structure deflection is electrically controlled. This means that the deflection should be maintained in the feedback loop by a deflection actuator, integrated with the mechanical part. This way, as the mass of the cantilever is quite small, the actuator induces structure movement with the highest energetic efficiency and

speed. Moreover, the actuation reliability is improved as the deflection of only the movable part is actuated. There are various electrical technologies for actuation of the cantilever displacement. The application of electrostatic actuation scheme is limited to cantilevers of big dimensions [2]. Moreover, it usually involves electrode biasing with relatively high voltage which is another limitation in MEMS technology. When a thin piezoelectrical film is deposited on the cantilever, the structure deflection can be piezoelectrically controlled [3]. However, the thin film increases the cantilever stiffness and, similarly to the electrostatic technology, the actuator is biased with higher voltage which hinders the applications in the integrated sensing systems. Displacement of the cantilever based MEMS devices can be actuated electrothermally as well [3]. In this case, a spring beam integrates a microheater. When the microheater is electrically biased, due to thermal expansion coefficients of various materials forming the cantilever, the entire structure starts to displace [4]. This way deflection in the frequency range of up to several MHz can be induced [5]. In the DC regime the cantilever can be displaced by even few micrometers [6]. The drawback of the electrothermally actuation scheme is that its application in liquids and consequently in biochemistry and biotechnology domains is limited. In this case, the heat generated in the microheater can propagate through the surrounding liquid and not only the beam structure itself, which significantly reduces the actuation efficiency. Moreover, in the electrothermal scheme the structure deflection can be controlled in one direction only. In contrast, the electromagnetic actuation technology is free from these drawbacks. In this technique the cantilever integrates a conductive loop called Lorentz loop. When an electromagnetical cantilever is electrically biased and when it is immersed in the magnetic field, electromagnetic force induces structure deflection [7].

The bidirectional cantilever deflection can be analysed basing on the model describing the electromagnetic force in Lorentz loop. The actuation force can be easily computed by means of the Lorentz force equation. The strong magnetic field in the range of fractions of a tesla can be induced by external magnets, the current in the loop can be biased by the low voltage electronics and the length of Lorentz loop can be determined with high accuracy. In this way DC and AC displacement can be controlled with highest precision, efficiency and reliability. Moreover, it is relatively straight forward to design systems operating at very low energy integrated with Application Specific Integrated Circuits (ASICs). The electromagnetic cantilever was introduced for the first time by Shen [8]. As the resonance structure can be observed with high resolution, they were also applied as high resolution magnetic field sensors [9, 10] and resonators [11].

The actuation precision and reliability were the main reasons, why the electromagnetic cantilevers were successfully applied in Scanning Probe Microscopy (SPM) [12, 13]. In all these investigations the cantilever deflection was determined metrologically (in other words quantitavely) which is of huge importance for the investigations of the interactions at a scanning probe microscopy tip.

The electromagnetic cantilever were also utilized in metrology of the mechanical stress associated with the adsorbtion of molecular self-assembled layers (Scanning Acoustic Microscope SAM) on the gold cantilever surface [14]. When thiol molecules adsorb (covalently bind) on the cantilever surface, mechanical stress occurs between molecular film and cantilever leading to the structure deflection. Such a response was usually used to detect (indicate qualitatively) with very high resolution the chemical surface reactions. But the electromagnetic force applied to compensate the deflection induced by the SAM cantilever enables us to quantitatively describe the recorded mechano-chemical phenomena for the first time. In the described experiments the electromagnetic cantilever was exposed to molecules, its deflection was observed and the bias current in Lorentz loop was controlled by an auxiliary proportional-integral (PI) controller.

Despite many advantages of the electromagnetic actuation, its limitations must be identified as well. To the most important problems, which must be taken into account, belong parasitic thermomechanical structure actuation when Lorentz loop is electrically biased. In this case, due to various coefficients of linear extension of the materials forming the spring beam, heat dissipated in

Peer-reviewed version available at Sensors 2018, 18, 2533; doi:10.3390/s18082533

the structure leads to additional structure deflection. In order to enable the structure deflection in the range of up to several micrometers the spring beam should exhibit low stiffness, which correlates with higher force and mass change detection resolution. Moreover, the resonance frequency of the designed and fabricated electromagnetic structures must be as high as possible, which makes it insensitive to the measurement disturbances and decreases the time response. The low stiffness and high resonance frequency can be achieved when the length and structure thickness are reduced in the appropriate way. However, in the case of the electromagnetic cantilevers one should also optimize the structure geometry in order to reduce Lorentz loop resistance. In this way the heat dissipated in the biased beam and the parasitic thermomechanical actuation are significantly reduced. Unfortunately, simple analysis of the equations modelling the electromagnetic cantilevers does not allow a closed-form design solution and only the optimal design methods make it possible to overcome the abovementioned limitations. In general, the methods of automated optimal design are based on repeated analysis to solve the field model [14], which ultimately influence the computational budget of the simulation.

The paper is organized as follows: in Section 2.1 and 2.2 forward and inverse models describing the behaviour of the cantilever are presented. In Section 2.3 the fabrication process is described.

In Sections 3.1 through 3.3 the optimization results are presented, while in Section 3.4 the measurement results are shown.

Finally, a discussion and conclusions are drawn.

2. Materials and Methods

2.1 Optimal design of an electromagnetically actuated cantilever: direct problem

The direct (or analysis) problem reads: given the shape g of the cantilever end, current I, and magnetic induction B, find:

the stiffness k of the cantilever;
the resonance frequency f of the cantilever;
the force F_z acting on the end region and its displacement Δz;
the electric resistance R (power-loss related) of the Lorentz loop.

The stiffness k of the cantilever can be calculated as follows:

$$k = \frac{Ebwt^3}{2b\left(L_1^3 - L_2^3\right) + 4wL_2^3} \quad [Nm^{-1}], \tag{1}$$

where E is the Young's modulus, b is the cantilever width, w the arm width, t is the thickness equal to 1.5 μm, L_1 is the cantilever length and L_2 is the tip length.
The resonance frequency f can be evaluated with the following approximated formula:

$$f \cong 0.161 \frac{t}{L_1^2}\sqrt{\frac{E}{\rho}} \quad [rads^{-1}], \tag{2}$$

where ρ is the mass density equal to 2330 kgm^{-3}.
The force F_z and its displacement Δz can be calculated as follows:

$$F_z = IbB, \tag{3}$$

$$\Delta z = \frac{F_z}{k}. \tag{4}$$

Eq. (3), which is derived form the Lorentz's equation, is under the assumption that the cantilever, i.e. the plane in which the current flows, is perpendicular to the magnetic induction field.
Finally, the electric resistance R can be calculated as the series of three electric resistances of the three path components (two arms, with the same resistance value R_1 and the tip, with resistance R_2):

$$R = 2R_1 + R_2 \cong 2\frac{\sigma^{-1}(L_1 - L_2)}{wt} + \frac{\sigma^{-1}b}{L_2 t}, \quad (5)$$

where σ is the electric conductivity of the boron-doped silicon (without metal layer) equal to $6.67\ 10^4\ Sm^{-1}$.

2.2 Optimal design of an electromagnetically actuated cantilever: inverse problem

If the shape of the cantilever end is defined by means of a n-dimensional vector $g = (g_1, ..., g_k, ..., g_n)$ of geometric variables (e.g. for a polygonally-shaped end region, the coordinates of the relevant vertices), the inverse (or design) problem reads: given current I and magnetic induction B, find the shape $g = (g_1, ..., g_k, ..., g_n)$ of the cantilever end region such that:

the stiffness k(g) of the cantilever is minimized;
the resonance frequency f(g) is maximized;
the displacement Δz(g) of the end region is maximized;
the electric resistance R(g) of the Lorentz loop is minimized.

A multi-objective optimisation problem characterized by four objective functions [k(g), f(g), Δz(g), R(g)] is originated. When more than one objective function is considered in the optimization, more solutions, belonging to the so-called Pareto front, are obtained. In particular, a solution is called Pareto optimal if there does not exist another solution that dominates it i.e. a solution that cannot be improved in any of the objectives without degrading at least one of the other objectives.
Considering n objective functions, a solution g_1 is said to dominate another solution g_2, if

$$f_i(g_1) \le f_i(g_2) \ \forall i \in (1,n) \quad \text{and} \quad (6)$$

$$\exists\, j \in (1,n) \ \text{such that} \ f_j(g_1) < f_j(g_2)\,. \quad (7)$$

A solutiong_1 is called Pareto indifferent with respect to a solution g_2 if

$$\exists\, j \in (1,n) \ \text{such that} \ f_j(g_1) < f_j(g_2) \ \text{and} \quad (8)$$

$$f_i(g_1) \le f_i(g_2) \ \forall i \ne j \in (1,n)\,. \quad (9)$$

When many objective functions (say more than two) are considered, it is very common to find solutions of the optimization problem which are indifferent in the Pareto sense to the starting point. However, these solutions are nevertheless interesting because they improve at least one objective function.

The shape of the cantilever is defined by four design variables, as shown in Fig. 1:

w, arm width
L_1, cantilever length
L_2, tip length
b, cantilever width.

Preprints (www.preprints.org) | NOT PEER-REVIEWED | Posted: 29 June 2018 doi:10.20944/preprints201806.0493.v1

Peer-reviewed version available at Sensors 2018, 18, 2533; doi:10.3390/s18082533

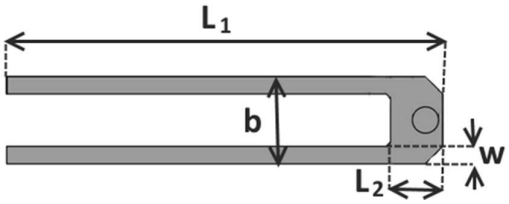

Figure 1. Design variables of the cantilever.

The variation range for each design variable is shown in Table 1.

Table 1. Variation range for the design variables (units in μm)

	w	**L1**	**L1**	**b**
Lower bound	20	100	50	100
Upper bound	-	600	100	150

In order to guarantee a geometrical congruency, the following constraint (units in μm) is set:

$$b \geq 2w + 10 . \quad (10)$$

Different optimizations are run, considering one (Opt1), two (Opt2) or more (Opt3) objective functions at a time:

Opt1 – each objective function i.e. k, f, Δz and R, is optimized in four different single-objective optimizations (Opt1k, Opt1f, Opt1z, Opt1R);

Opt2 – the following optimizations are run: k and R are optimized (Opt2kR), f and z are optimized (Opt2fz), f and R are optimized (Opt2fR), z and R are optimized (Opt2zR);

Opt3 – k, z and R are optimized (Opt3).

In order to solve these optimization problems, an evolutionary algorithm of lowest order is applied [15]. This algorithm is able to solve single-objective problems (in this case it is called "ESTRA method" [16,17]) and multi-objective problems ("MOESTRA method" [18]). The search in the design space begins in a region of radius d_0 (standard deviation) centered at the initial point m_0 (mean value); m_0 is externally provided, while d_0 is internally calculated on the basis of the bounds boxing the variation of the design variables.

Setting $m = m_0$ and $d = d_0$, the *generation* of the design vector $x = m + u\,d$ then proceeds, resorting to a normal sample $u \in (0,1)$. It is verified that x fulfils bounds and constraints (i.e. that x is feasible), otherwise a new design vector is generated until it falls inside the feasible region.

The associated objective function f(x) is then evaluated and the test if f(x) dominates f(m) (eqs. 6-7) is performed; if the test is successful, m is replaced by x (the so-called *selection* process), otherwise m is retained.

The next step is concerned with the size of the search region that will be used for the successive iteration. The underlying rationale is that when a point better than the current one is found, the radius of the search region is increased around the new point to search for further improvements; if no improvement is found, the radius of the search region is gradually decreased up to convergence (*annealing* process).

In this respect, the evolutionary algorithm substantially differs from a deterministic one e.g. Nelder & Mead algorithm [19], in which the search region would be narrowed around the better point in

order to converge towards the corresponding, nearest minimum. The drawback is that this minimum might be a local one. On the contrary, the evolutionary algorithm, if successful in finding a better point, covers a larger region of search in order to see if there would be another good candidate in the neighborhood, and then does the opposite when this is not deemed possible. This way, there is a non-zero probability of finding the region where the global optimum of the objective function is located.

To assess the optimization results, a set of prototypes has been fabricated based on the technology described in the subsequent Section.

2.3. Fabrication process

The fabrication process of the microcantilevers used for a radiation pressure sensing based on a double side micromachining concept [20]. However, in contrast to the typical technology based on bulk silicon substrates, in this case the SOI wafers with 1 and 1.5 micrometres thick buried oxide and device layer respectively were used as the input material. Despite the fact that the use of SOI substrates is more expensive, this solution has many advantages compared to the use of the bulk wafers. Two advantages of using the SOI substrates are particularly important.

The first advantage is a significant simplification of the microcantilever production process. The second advantage is a guarantee that all cantilevers defined on one wafer are characterized by uniform thickness regardless of its shape and size (the thickness depends only on the SOI wafer device layer properties).

Therefore, using the SOI substrate, the production technology consists of only four technological steps: high p doping of the whole device layer, definition of a gold contacts and mirrors, definition of the shape of the cantilever and finally the releasing of the structures. Fig. 2 presents the SEM image of the cantilever after three steps, i.e. after plasma etching processes. On the magnification (Fig. 2b and c) the four layers can be observed: gold (serve as a mirror), 1.5 μm silicon layer, buried silicon dioxide and handle silicon wafer.

Preprints (www.preprints.org) | NOT PEER-REVIEWED | Posted: 29 June 2018 doi:10.20944/preprints201806.0493.v1

Peer-reviewed version available at Sensors 2018, 18, 2533; doi:10.3390/s18082533

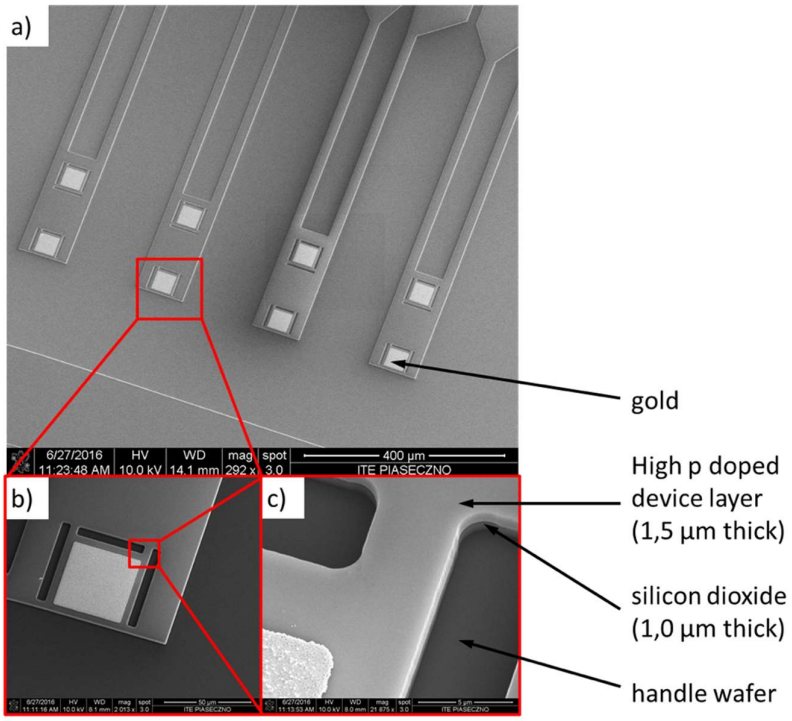

Figure2. the SEM image of the cantilever matrix after three technological steps (inter-operative control).

On the Fig. 3 the example final cantilevers matrix after released operation is presented.

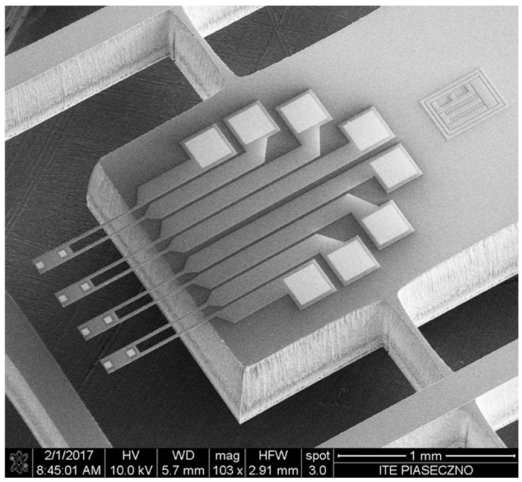

Figure 3. The final structure.

Presented construction were optimized for magnetoelectric method of actuation first proposed by Buguin group [21]. The use of SOI wafers guaranteed a homogeneous doping of the device layer, which significantly reduced the thermal actuation effect. The homogeneous, high p doped device layer were obtained by using boron doped layers deposited by LPCVD method [22]. On the Fig. 4 our boron dopant profile simulation results are presented. The simulation confirmed that the boron dopant profile is on the same level along the entire device layer thickness and in that case the thermal expansion coefficient should be also constant [23].

Preprints (www.preprints.org) | NOT PEER-REVIEWED | Posted: 29 June 2018 doi:10.20944/preprints201806.0493.v1

Peer-reviewed version available at Sensors 2018, 18, 2533; doi:10.3390/s18082533

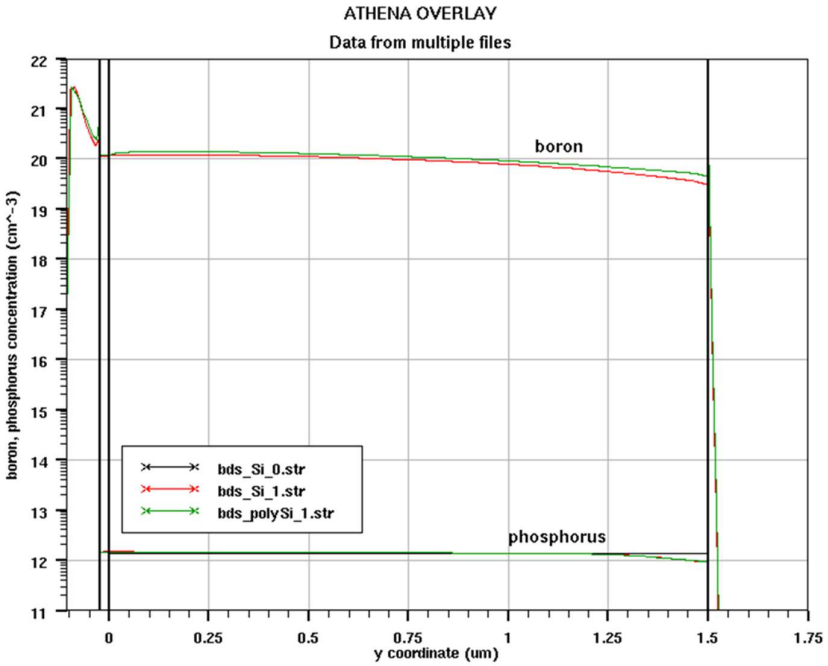

Figure 4. The high p dopant of the SOI device layer simulation result.

3. Results

3.1. Single-objective optimization results

The results of the single-objective optimizations are shown in Table 2. In each table the values of the design variables and of the functions (k, f, Δz, R) are shown. In particular, the minimized objective function is highlighted in bold.

Table 2. Single-objective optimization Opt1k results.

	w [μm]	L_1 [μm]	L_2 [μm]	b[μm]	k [Nm^{-1}]	f [kHz]	Δz [nm]	R [Ω]
Initial	20	500	50	100	$4.32\ 10^{-2}$	8	925.37	470
Opt1k	21.05	568.92	53	114.39	**$3.09\ 10^{-2}$**	6.18	1481.94	511.84
Opt1f	24.55	210.26	64.57	122.56	0.726	**45.26**	67.56	137.67
Opt1z	22	567.57	63.93	127.90	$3.25\ 10^{-2}$	6.21	**1573.71**	478
Opt1R	47.59	210.51	80.73	119.47	1.39	45.16	34.29	**69.34**

From Table 2 - Opt1k, it can be noted that the non-controlled objective functions f decreases, which is unwanted, Δz increases (desiderable) and R increases (unwanted).

From Table 2 - Opt1f, it can be noted that the non-controlled objective functions k increases, which is unwanted, Δz decreases (unwanted) and R decreases (desiderable).

From Table 2 - Opt1z, it can be noted that the non-controlled objective functions k decreases (desiderable), f decreases (unwanted) and R increases (unwanted).

From Table 2 - Opt1R, it can be noted that the non-controlled objective functions k increases (unwanted), f increases (desiderable) and Δz decreases (unwanted).

3.2. Bi-objective optimization results

The results of the bi-objective optimizations are shown in Table 3. In each table the values of the design variables and of the functions (k, f, Δz, R) are shown. In particular, the minimized objective functionsare highlighted in bold.

Preprints (www.preprints.org) | NOT PEER-REVIEWED | Posted: 29 June 2018 doi:10.20944/preprints201806.0493.v1

Peer-reviewed version available at Sensors 2018, 18, 2533; doi:10.3390/s18082533

Table 3. Bi-objective optimization results.

	w [μm]	L_1 [μm]	L_2 [μm]	b[μm]	k [Nm^{-1}]	f [kHz]	Δz [nm]	R [Ω]
Initial	20	500	50	100	$4.32\ 10^{-2}$	8	925.37	470
Opt2kR	24.05	557.13	62.33	110	**$3.76\ 10^{-2}$**	6.45	1170.59	**429.13**
Opt2fz	21	490.14	55.40	136.12	$4.82\ 10^{-2}$	**8.33**	**1129.24**	438.48
Opt2fR	60.92	210.04	86.10	135.02	1.79	**45.36**	30.29	**56.37**
Opt2zR	27.17	568.93	57.71	110.96	$3.99\ 10^{-2}$	6.18	**1113.33**	**395.46**

From Table 3 - Opt2kR, it can be noted that the non-controlled objective function f decreases, which is unwanted, but Δz increases (desiderable).

From Table 3 - Opt2fz, it can be noted that the non-controlled objective function k increases, which is unwanted, but R decreases (desiderable).

From Table 3 - Opt2fR, it can be noted that the non-controlled objective function k increases (unwanted) and Δz decreases (unwanted).

From Table 3 - Opt2zR, it can be noted that the non-controlled objective function k decreases (desirable) and f decreases (unwanted).

3.3. Tri-objective optimization results

The results of the tri-objective optimization are shown in Table 4. The values of the design variables and of the functions (k, f, Δz, R) are shown. In particular, the minimized objective functions are highlighted in bold.

Table 4. Tri-objective optimization Opt3 results.

	w [μm]	L_1 [μm]	L_2 [μm]	b[μm]	k [Nm^{-1}]	f [kHz]	Δz [nm]	R [Ω]
Initial	20	500	50	100	**$4.32\ 10^{-2}$**	8	**925.37**	**470**
Final	23.97	562.15	68.13	111.78	**$3.65\ 10^{-2}$**	6.33	**1226.19**	**428.66**

From Table 4, it can be noted that the non-controlled objective function f decreases, which is unwanted.

From the practical viewpoint, the solutions found in Opt2fz and Opt3 are felt to be the best ones, as explained in the following Section 3.2. Hence these cantilevers, as well as the initial cantilever, were fabricated and measured to verify the design and assess the optimization results.

3.4. Measurements on optimal cantilevers

The cantilevers according to the initial design as well as of the shapes obtained from Opt2fz and Opt3 optimizations were considered to be optimal. With Opt2fz solution, significant increase in deflection and small decrease in resistance of loop were obtained. These two changes were most desirable and came without deterioration in the resonant frequency. Another solution considered to be optimal, the Opt3, exhibits even higher deflection and smaller resistance at the cost of 15% lower frequency. These two cantilevers were fabricated and finally measured. The example array is shown in Fig. 5a. This manufactured cantilever array consists of four cantilevers, in particular:

- two cantilevers corresponding to initial design,
- final design, according to Opt2fz optimization result
- final design, according to Opt3 optimisation result

a) b)

Preprints (www.preprints.org) | NOT PEER-REVIEWED | Posted: 29 June 2018 doi:10.20944/preprints201806.0493.v1

Peer-reviewed version available at Sensors 2018, 18, 2533; doi:10.3390/s18082533

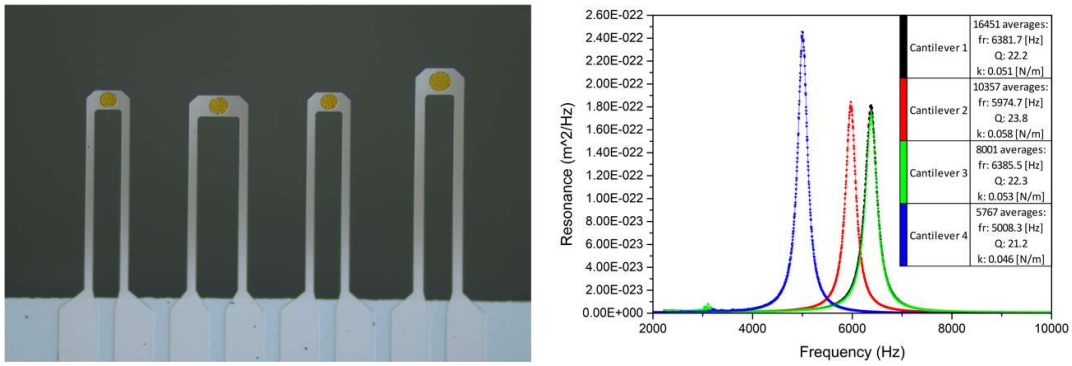

Figure 5.(**a**) example of manufactured cantilever array consisting of four cantilevers. Cantilevers 1 and 3 (from left to right) correspond to the initial design, while 2 and 4 are the optimal cantilevers afteroptimizations Opt2fz and Opt3. (**b**) the resonance response of the manufactured cantilevers.

To verify their properties, we have measured the thermomechanical noise of the cantilevers. The power spectrum of each resonant mode in the thermomechanical noise is defined by the formula:

$$X_{th}(f) = 2k_B T\pi^{-1}Q^{-1}f_0^3 k^{-1}[(f_0^2 - f^2)^2 + f_0^2 f^2 Q^{-2}]^{-1}, \quad (11)$$

where f is the cantilever resonant frequency, Q is the quality factor, k is the spring constant of the cantilever, k_B is the Boltzmann constant, T is the absolute temperature. By fitting parameters of eq. (11) to the measurements, the mechanical parameters are obtained. The thermomechanical noise formula is a result of the equipartition theorem [24]. Due to this theorem an object, which dissipates energy in thermal equilibrium, is subject to a fluctuation force. The measured resonance responses of the cantilevers shown in Fig. 5a are shown in Fig. 5b.

Two cantilever arrays, each of which containing twice the same initial design cantilever, were fabricated. The measurement was then performed for both cantilever arrays, hence for four cantilevers (Table 5). This measurement provides information about the cantilever resonant frequency and its stiffness. Additionally, the resistance of the loop was measured. The cantilever provides direct electrical contacts. The Keithley 2000 multimeter was used to measure the resistance of the loop. The measurement was conducted in DC mode. The Keithley multimeter applies a 100 μA current and subsequently the voltage drop was measured. The results of manufactured cantilever arrays according to initial design are shown in Table 5.

Table 5. Measurements on the initial cantilever.

Measured quantities			Computed quantities			
R [Ω]	f [kHz]	Q	k [Nm^{-1}]	F_{min}[pN]	I_{min}[nA]	P_{min}[fW]
1.89	6382	22.2	0.051	0.308	9.63	175.2
2.26	6386	22.3	0.053	0.313	9.79	216.6
1.88	6632	23.4	0.060	0.319	9.98	187.2
2.26	6634	23.4	0.065	0.306	9.55	206.2

The cantilever parameters manufactured according to Opt2fz and Opt3 optimisation results are provided in Table 6.

Table 6. Measurements on the Opt2fz and Opt3 cantilever.

Peer-reviewed version available at Sensors 2018, 18, 2533; doi:10.3390/s18082533

	Measured quantities			Computed quantities			
	R [Ω]	f [kHz]	Q	k [Nm^{-1}]	F_{min}[pN]	I_{min}[nA]	P_{min}[fW]
Opt2fz,array1	2.16	5975	23.8	0.058	0.328	7.13	109.8
Opt2fz,array2	2.15	5819	25.3	0.063	0.336	7.30	114.7
Opt3,array1	1.74	5008	21.2	0.046	0.338	9.60	160.4
Opt3,array2	1.74	5205	22.3	0.038	0.294	8.35	121.23

4. Discussion

The measured results of the initial cantilever slightly differ to those calculated for the initial prototype in Tables 2-4. In fact, the manufactured cantilevers contain the gold layer at each end. This gold is supposed to improve reflection of the laser beam from cantilever surface in AFM measurements. The resonant frequency differs due to the mass of the added gold layer. The resulting frequency of the manufactured cantilevers is lower and equal to approximately 6.5 kHz. It should be also noted that, due to the many technological processes required to manufacture the cantilevers, some drifts in measured parameters are unavoidable. This can be particularly seen for the initial cantilever, where we can compare results for four manufactured pieces and parameters of each of them differ.

The main difference between the optimization results and manufactured cantilevers is the value of the resistance. It comes out from the fact that the value of doping concentration in the manufactured cantilevers is lower than the assumed one in the optimization procedure. However, this discrepancy does not affect the optimisation results and its assessment (as it only influences material property).

Provided that all the optimization runs start from the same initial point, the following remarks can be put forward.

The solutions obtained in Opt1k, Opt1f, Opt1z and Opt1R differ in both design vector (w, L_1, L_2, b) and objective vector (k, f, Δz, R). This proves that a single solution simultaneously satisfying all the design criteria does not exist. From the optimisation theory viewpoint, it is a design conflict problem that can be studied via Pareto optimality.

Solutions obtained in Opt2 and Opt3 can be considered Pareto-equivalent to the initial one, because three objectives improve, while one objective deteriorates (e.g. solution of Opt3 where k, Δz and R improve, while f deteriorates). From the application viewpoint, provided the amount of deterioration in one objective is acceptable, Pareto-equivalent solutions may represent a good alternative to the initial solution.

5. Conclusions

A class of electromagnetically actuated cantilevers has been considered. Their optimal shape design has been carried out by means of a multi-objective design method, based on evolutionary algorithm. The subsequent fabrication of cantilever arrays and relevant measurements have assessed the optimization results. This puts the ground for a more general procedure of cantilever design for nanometrology purpose.

Acknowledgments: The fabrication and measurements of the electromagnetic actuation were done within the NCN OPUS 9 Grant - "Metrology of molecular interactions using electromagnetically actuated MEMS force sensors-MetMolMEMS" (Grant No. 2015/17/B/ST7/03876).

Author Contributions: Paolo Di Barba conceived and formulated the optimal design problem, run the optimization procedure and analyzed the results. Teodor Gotszalk wrote the introduction of the article. Karolina Orłowska and Wojciech Majstrzyk measured the cantilevers and analysed the measurement data. They also prepared the measurement results chapter. Maria Evelina Mognaschi contributed to the analysis of the optimization results and the discussion. She also wrote the paper. Slawomir Wiak read subsequent versions of the paper and contributed to the bibliographic references. Andrzej Sierakowski prepared the technological process and manufactured the cantilevers. He was also responsible for preparing chapter of the manufacturing process.

Conflicts of Interest: The authors declare no conflict of interest.

References

1. Lang, H.P.; Hegner, M.; Gerber, C. Nanomechanical cantilever array sensors. In *Springer Handbook of Nanotechnology*. Springer: Berlin, Heidelberg, 2013, pp. 457-485.
2. Gaspar, J.; Chu, V.; Conde, J.P. Electrostatic actuation of thin-film microelectromechanical structures. *J. Appl. Phys.* 2003, 93, pp. 10018–10029. doi:10.1063/1.1573344.
3. Minne, S.C.; Manalis, S.R.; Quate; C.F. Parallel atomic force microscopy using cantilevers with integrated piezoresistive sensors and integrated piezoelectric actuators, *Appl. Phys. Lett.*, 1995, 67. doi:10.1063/1.115317
4. Angelov, T.; Roeser, D.; Ivanov, T.; Gutschmidt, S.; Sattel, T.; Rangelow, I.W. Thermo-mechanical transduction suitable for high-speed scanning probe imaging and lithography, *Microelectron. Eng.* 2016, 154, pp. 1–7. doi:10.1016/j.mee.2016.01.005.
5. Woszczyna, M.; Zawierucha, P.; Pałetko, P.; Zielony, M.; Gotszalk, T.; Sarov, Y.; ... & Rangelow, I. W. Micromachined scanning proximal probes with integrated piezoresistive readout and bimetal actuator for high eigenmode operation. *Journal of Vacuum Science & Technology B, Nanotechnology and Microelectronics: Materials, Processing, Measurement, and Phenomena*. 2010, 28(6).
6. Majstrzyk, W.; Ahmad, A.; Ivanov, T.; Reum, A.; Angelow, T.; Holz, M.; ... & Rangelow, I. W. Thermomechanically and electromagnetically actuated piezoresistive cantilevers for fast-scanning probe microscopy investigations. *Sensors and Actuators A: Physical*. 2018, *276*, pp. 237-245.
7. Nieradka, K.M; Kopiec, D.; Małozięć, G.; Kowalska, Z.; Grabiec, P.; Janus, P.; ... & Gotszalk, T. Fabrication and characterization of electromagnetically actuated microcantilevers for biochemical sensing, parallel AFM and nanomanipulation. *Microelectronic Engineering*. 2012, 98, pp. 676-679.
8. Shen, B.; Allegretto, W.; Hu, M.; Robinson, A. Cmos micromachined cantilever-in-cantilever devices with magnetic actuation, *Electron Device Letters, IEEE*. 1996, 17(7), pp. 372–374.
9. Adhikari, R.; Kaundal, R.; Sarkar, A.; Rana, P.; Das, A.K. The cantilever beam magnetometer: A simple teaching tool for magnetic characterization. *American Journal of Physics. 2012,* 80(3), pp. 225–231.
10. Hsieh, C.H.; Dai, C.L.; Yang, M.Z. Fabrication and characterization of cmos-mems magnetic microsensors, *Sensors*. 2013, 13(11), pp. 14728–14739.
11. Rhoads, J.F.; Kumar, V.; Shaw, S.W.; Turner, K.L. The non-linear dynamics of electromagnetically actuated microbeam resonators with purely parametric excitations. *International Journal of Non-Linear Mechanics*. 2013, 55, pp. 79–89.
12. Somnath, S.; Liu, J. O.; Bakir, M.; Prater, C. B.; King, W. P. Multifunctional atomic force microscope cantilevers with Lorentz force actuation and self-heating capability. *Nanotechnology*. 2014, 25(39).
13. Majstrzyk, W.; Mognaschi, M. E.; Orłowska, K.; Di Barba, P.; Sierakowski, A.; Dobrowolski, R.; Grabiec, P.; Gotszalk, T. Electromagnetic cantilever reference for the calibration of optical nanodisplacement systems. *Sensors and Actuators* (under revision).
14. Di Barba, P.; Mognaschi, M.E.; Venini, P.; Wiak, S. Biogeography-inspired multiobjective optimization for helping MEMS synthesis. *Archives of Electrical Engineering*, 2017, 66 (3), pp. 607-623.
15. Di Barba, P. *Multiobjective Shape Design in Electricity and Magnetism*. Springer-Verlag: Berlin, Germany, 2010.
16. Di Barba, P.; Savini, A.; and Wiak, S. *Field Models in Electricity and Magnetism*. Springer: Berlin, Germany, 2008.
17. Di Barba, P., Mognaschi, M.E.; Lowther, D.A.; Sykulski, J.K. A benchmark TEAM problem for multi-objective pareto optimization of electromagnetic devices. *IEEE Trans. on Magnetics*, 2018, *54*(3).
18. Di Barba, P.; Mognaschi, M.E. Industrial design with multiple criteria: Shape optimization of a permanent-magnet generator. *IEEE Trans. on Magnetics*, 2009, 45 (3), pp. 1482-1485.
19. Costamagna, E.; Di Barba, P.; Mognaschi, M.E.; Savini, A. Fast algorithms for the design of complex-shape devices in electromechanics. In *Studies in Computational Intelligence*, Springer: Berlin, Germany, 2010; Volume 327, pp. 59-86.
20. Gotszalk, T.; Grabiec, P.; Rangelow, I. W. Piezoresistive sensors for scanning probe microscopy. *Ultramicroscopy*. 2000, Vol. 82, pp. 39-48.

21. Buguin, A.; Du Roure O.; Sliberzan, P. Active atomic force microscopy cantilevers for imaging in liquids. *Applied Physics Letters*. 2001, pp. 2982-2984.
22. Węgrzecki, M.; Wolski, D.; Bar, J.; Budzyński, T.; Chłopik, A.; Grabiec, P.; Kłos, H.; Panas, A.; Piotrowski, T.; Słysz, W.; Stolarski, M.; Szmigiel, D.; Węgrzecka, I.; Zaborowski, M. 64-element photodiode array for scintillation detection of x-rays. Proc. SPIE 9291, 13th International Scientific Conference on Optical Sensors and Electronic Sensors, 19 August 2014; doi: 10.1117/12.2069837; http://dx.doi.org/10.1117/12.2069837
23. Rueda, H.A.; Law, M.E. Modeling of Strain in Boron-Doped Silicon Cantilevers. Technical Proceedings of the 1998 International Conference on Modeling and Simulation of Microsystems, ISBN: 0-96661-35-0-3, pp. 94 – 99.
24. Butt, H.J.; Jaschke, M. Calculation of thermal noise in atomic force microscopy. *Nanotechnology*. 1995, 6, pp. 1–7,